15 September 2022
philip.geissler@cern.ch

Varactor Boards, HV Connections & BASE Upkeep

Philip Geißler

Keywords: CERN Summer Student Programme 2022, CERN Summer Students Project Notes, BASE

Summary: RIKENs BASE experiment aims to measure possible differences in specific charge and g-factor between Protons and Antiprotons as an avenue to probing for CPT violation. In the advanced penning trap setup which measures these quantities, resonators oscillate at specific frequencies tunable via a varactor circuit, and catching electrodes need to be supplied with high voltage without interaction with other components. In implementing improvements, work on opening and closing the experiment needs to be done. This document will focus on these three topics and my contribution during the summer student programme.

Contents

1 Introduction

1.1 Charge-to-Mass Ratio, Magnetic Moment and BASEs Goals

BASE tests CPT invariance by looking for differences in charge-to-mass ratios and magnetic moments of protons and antiprotons via their behaviour in a magnetic field.

$$\omega_c = \frac{q}{m}B, \qquad \omega_L = \frac{g}{2}\frac{q}{m}B \qquad \Longrightarrow \qquad \frac{q}{m} = \frac{\omega_c}{B}, \qquad g = 2\frac{\omega_L}{\omega_c} \tag{1}$$

As shown in equation 1, the charge-to-mass ratio and g-factor of a particle in a constant magnetic field only depends on its cyclotron frequency ω_c and Larmor frequency ω_L. As particles need to be confined in all directions, Penning traps are used which confine the particle along the magnetic field via an electric potential. This causes an axial, magnetron and modified cyclotron mode to form instead $(\omega_z, \omega_-, \omega_+)$. Each of those frequencies causes surface currents on adequately shaped electrodes. These currents can be amplified and measured directly with resonators [1]. For frequencies outside of achievable resonator specifications, sideband coupling can be used to measure them via their interaction with another mode. The Brown-Gabrielse invariance Theorem

$$\omega_c^2 = \omega_+^2 + \omega_z^2 + \omega_-^2 \text{ [2]}$$

can subsequently be used to calculate the free cyclotron frequency, even for misaligned Penning traps.

The Larmor frequency ω_L can't be measured directly via surface currents, so another approach is used. A particle in a constant magnetic field in the particle reference frame, oriented perpendicular to the spin direction flips spin states over time [3]. Moving from the particle reference frame to the lab reference frame transforms this constant magnetic field into a circularly polarized wave perpendicular to the quantization axis (the main trap magnetic field) with the frequency of spin precession, ω_L. An EM-wave at the Larmor frequency, radiated into the trap, therefore leads to spin flips. Frequencies close to ω_L can still cause spin flips, with decreasing efficiency for larger deviations [3]. One can consequently drive at different frequencies multiple times and maximize spin flip probability to obtain the Larmor frequency. To detect spin states, a magnetic bottle is introduced into of the BASE Penning traps . This changes the potential well and produces non-degenerate energy levels of the spin up and spin down state.

$$\Delta\Phi_{\text{well}} = -\mu\vec{B}(z) = -\mu\frac{\mathrm{d}^2B}{\mathrm{d}z^2}z^2 + \mathcal{O}(z^4) \qquad \Longrightarrow \qquad \omega_{z,\text{Bottle}} = \sqrt{\omega_z^2 \pm \frac{2\mu_{\bar{p}}}{m_{\bar{p}}}\frac{\mathrm{d}^2B}{\mathrm{d}z^2}}$$

The state can thus be detected by their different resonance frequencies. Spin states can be determined by broadband driving a spin flip. If the frequency increases post-flip, the spin increased, so the particle is now in the spin up state. Now the timed drive at a specific frequency can happen. As protons and antiprotons are particles with a spin of $\frac{1}{2}$, they only have two spin states and can therefore only increase in spin once consecutively. So if a particle spin increase is seen again during the broadband drive afterwards, then a spin flip in the other direction must have occurred during the timed drive [4],

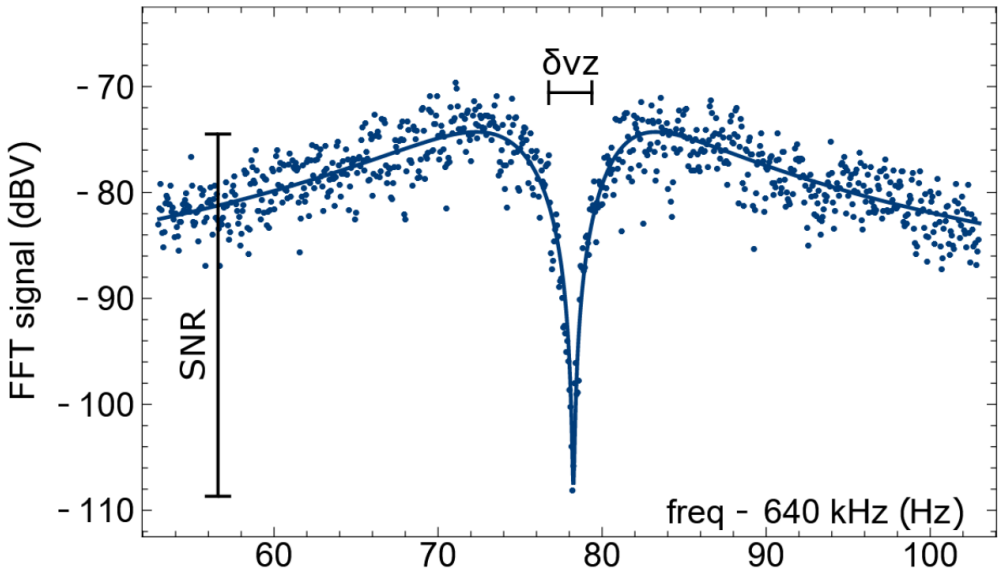

Figure 1: Noise density dip due to a particle. Image taken from [4], which also gives a detailed theoretical description of this effect.

1.2 Resonators

The surface currents from the particle motion addressed above are only a few fA and thus too small to be measured directly. However, one can introduce AC currents into the electrode and analyze the damping behaviour. Driven at resonance frequency, the particle acts as energy storage, converting it into kinetic energy. This effect decreases as the driving frequency moves away from resonance, and more energy is absorbed and converted to heat via setup resistances. Johnsson noise around the resonance frequency can consequently be used to detect a particle, as the particle absorbs the resonance frequency component, leading to suppressed voltages at those frequencies. As the resonance frequency phase of the Noise is uniformly randomly distributed, no net energy absorption of the particle occurs above thermal equilibrium, as the constructive and destructive drive phases cancel each other out. At BASE, a high-Q parallel RLC circuit in parallel with the electrode-particle system and RLC resonance frequency at particle resonance frequency is used. This leads to high noise power density around the resonance frequency due to the high RLC impedance, which gets shorted in a very narrow frequency range by the particle, appearing as a sharp dip as shown in fig. 1.

Sometimes the resonator noise at the particle resonance frequency should be removed, i.e. to reduce heating rates of a particle colder than the environment. Other times, the resonator resonance frequency needs to be shifted, i.e. because the antiproton and H^- ion resonate at different frequencies if trapped at the same potential due to their slightly different masses, or because the potential well deepens or changes curvature. One solution is to add a switch into the setup which can disable the resonator and add one resonator for each relevant frequency, but space and complexity constraints speak against it. Instead, by varying the RLC capacitance or inductance, the resonance frequency can be changed, detuned and adapted to changing potential wells when needed without the need for multiple resonators. A

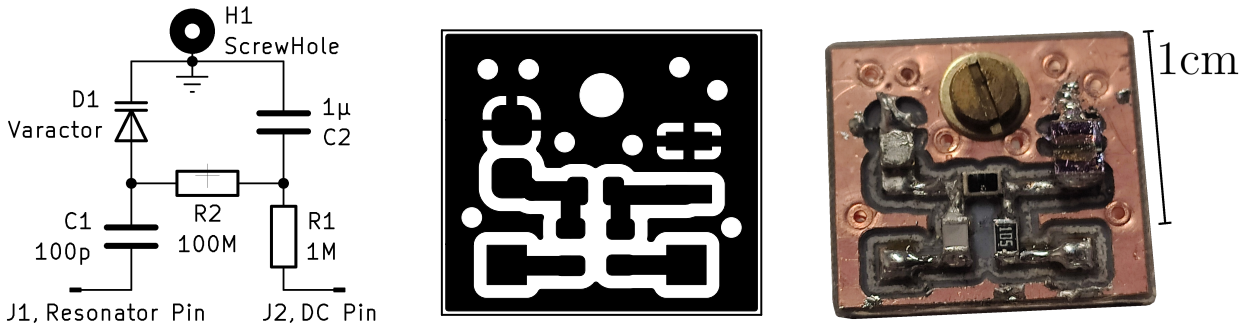

Figure 2: Varactor board schematic, pcb layout and image of final product.

varactor board can do this via the application of a DC bias voltage from the outside of the closed experiment. It also allows measuring the dip in fig. 1 and thus the particle oscillation frequency at different levels of particle to resonator oscillation detuning. It was found in previous measurement campaigns that such detuned measurements can lead to different fitted resonant particle frequencies of around 30ppt, even when taking account of the changing dip shapes. So with the varactor board it is possible to eliminate such uncertainties by showing that such frequency changes do not occur at changing amounts of detuning.

1.3 HV Electrodes

The Antiprotons for BASE are provided by the collisions of accelerated protons with the Antiproton Decelerator target and subsequently by the decelerator itself, ELENA and a degrader foil. Afterwards, some of the antiprotons have an energy below some keV and are able to be trapped in a kilovolt range potential well between two well timed high voltage electrodes. As the antiprotons need to be able to be easily transferred into other specialized traps after some further cooling, the HV electrodes are placed directly next to the trap stack in the most central, coldest and highest vacuum part of the experiment. They need to be pulled to the correct potential at the correct time by cables through the experiment and switches of the experiment. Before ELENA, arriving antiprotons had higher energy and thicker degrader foils were used. With the necessary thinner foil the energy distribution of transmitted antiprotons is different now and may require deeper potential wells for catching. Thus its useful to know and possibly improve the maximum energy catching cutoff. This necessitated engaging with a HV power source, testing all components for electrical breakdown and the HV switch for its behaviour.

2 Varactor Board

A varactor is a diode operated in reverse direction and optimized so that the depletion of the doped region via an applied voltage leads to large changes in capacitance C_V. By capacitively decoupling the varactor from a circuit and applying a variable DC voltage, it can be used as a tunable capacitance without the DC component interfering in the circuit. DC voltage would

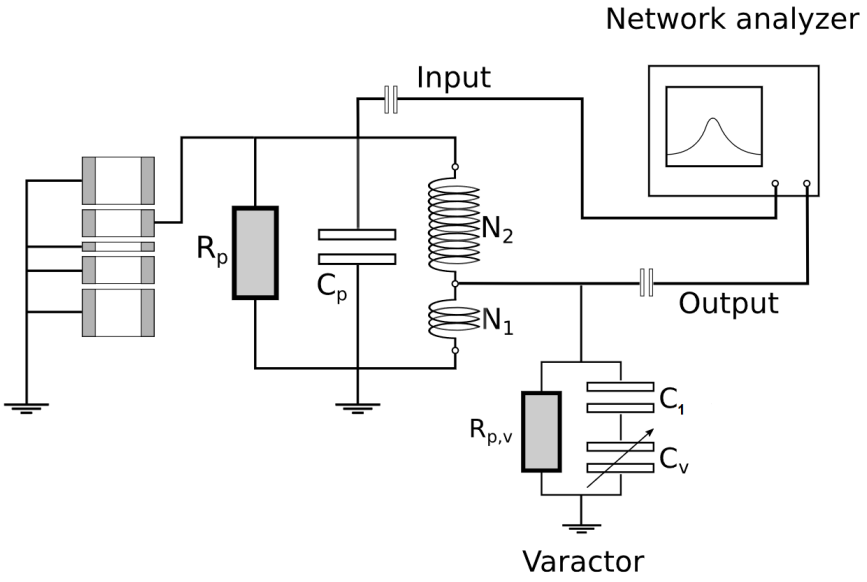

Figure 3: Particle detection setup tunable via varactor. Taken from [5].

partially pull up the connected electrode in the trap, changing the potential well, ruining precision and possibly releasing the particles. Such a setup is shown in fig. 2. J1 is the circuit connection, J2 the DC biasing connection, and the whole setup acts as a capacitance $C_{\text{setup}} = C_1 \parallel C_V(U_{J2})$ to ground. If the varactor setup is subsequently introduced into the particle detector as in fig. 3, the RLC resonance frequency can be shifted via the DC biasing voltage. With the tap fraction $\kappa = N_1/(N_1 + N_2)$, it can be calculated as

$$\omega_{\text{resonance}} = \frac{1}{\sqrt{L_{RLC} C_{\text{total}}}} \qquad C_{\text{total}} = C_{RLC} + \left[C_1 \parallel C_V \kappa^2\right] \qquad [5,\ 6].$$

One of my projects entailed building such a varactor setup for our precision trap (PT) axial detector, one of the resonators used for particle detection and measurement. Currently, it roughly has a resonance frequency of 640 kHz, a total capacitance of 31 pF, an inductance of 2 mH and a quality factor of roughly 30 000. With a resonance bandwidth in the 10 Hz to 100 Hz range, and 356 Hz changes between antiprotons and H^- ions due to their 0.1% difference in specific charge ($\omega_z \propto (\frac{q}{m})^{1/2}$), tunability of at least a kilohertz is needed. More if the trap potential is also getting changed. With a tap fraction of less than 8.6% and infinite capacitive DC decoupling, the Macom MA46H072 and MA46H073 with a capacitance range of 1.2 pF to 7.9 pF and 1.9 pF to 13.5 pF respectively are able to tune the resonance frequency in a range of more than 100 kHz each, which is sufficient for our purpose. A decoupling capacitor with $C_1 = 100$ pF shrinks this range by less than 10%, which is acceptable. Special care needs to be taken so that the setup is compatible with cryogenic temperatures and high vacuum. Table 1 lists all components used in the circuit in fig. 2.

To characterize the varactor board via the resonance frequency change, the resonator itself needs to be characterized first. This can be done by connecting it to a network analyzer directly, and with a reference capacitance C_r in parallel (in series to ground).

Table 1: Varactor board component reference

Element	Component	Note
Varactor, D1	MA46H072-1056 / MA46H073-1056	
R1	ERA6AEB105V	
R2	RH73H2A100MKTN	
C1	251R15S101JV4S	NP0 temperature characteristic
C2	ECPU1C105MA5	C decreases with temperature
Screw, H1	Brass M2 Screw	acts as ground connection
Substrate	Diclad 870/880 Laminate	low loss tangent

$$\omega_0 = \frac{1}{\sqrt{L_{RLC} \cdot C_{RLC}}} \qquad \omega_{C_r} = \frac{1}{\sqrt{L_{RLC} \cdot (C_{RLC} + C_r)}} \qquad \Longrightarrow \qquad L_{RLC} = \frac{1}{C_r} \cdot \left(\frac{1}{\omega_{C_r}} - \frac{1}{\omega_0^2} \right) \qquad C_{RLC} = C_r \cdot \frac{\omega_{C_r}^2}{\omega_0^2 - \omega_{C_r}^2}$$

Afterwards, the $f(U)$ and $Q(f)$ curves can be measured and the varactor characteristics determined numerically, leading to the results in fig. 4 for room temperature measurements.

As can be seen, the measurements agree well with the specifications from the data sheet, and it seems that the data sheet just interpolated between four measured points at 0.1 V, 1 V, 10 V and 20 V in the log-log space. The measurements were redone in a vacuum test setup with a cold head at around 3 K and after some problems with the MA46H072-1056 changing behaviour at higher voltages, the MA46H073-1056 was chosen. Its measurements are given in fig. 5. As able to be seen in the $f(u)$ plot, the resonator is able to be tuned between 2.370 MHz and 2.406 MHz, with quality factors around 40000. In contrast, the free resonator achieved a Quality factor of 60 000(1000), which equates to a parallel resistance of 430(20) MΩ. Modeled as an extra parallel resistor, the varactor board would have a resistance of 450 MΩ to 1150 MΩ, depending on DC bias, to pull the resonator to the Quality factor of 40000.

With the lower temperature, problems at higher voltages seem to occur. The quality factor diminishes at 20 V and the network analyzer signal becomes very noisy. At low voltages, the varactor behaviour starts to differ from a perfect capacitance and the resonance curve exhibits positive skewness. As the varactor board was soldered to the trap resonator without further changes after the characterization, it is advised to use the board with bias voltages of 0.5 V to 15 V to circumvent both of these issues. Fig. 6 shows the behaviour of the MA46H073-1056 Varactor board soldered to the BASE precision trap. Some resonant side band frequencies can be seen and the quality factor has lowered to roughly 14000 due to the different resonator. The resonance frequency was able to be tuned from 630 kHz to over 645 kHz, even making use of up to −1 V of forward voltage not tested in the cold head. With the signal-to-noise ratio in the setup used for the experiment staying around 24 to 25 over the whole tuning range.

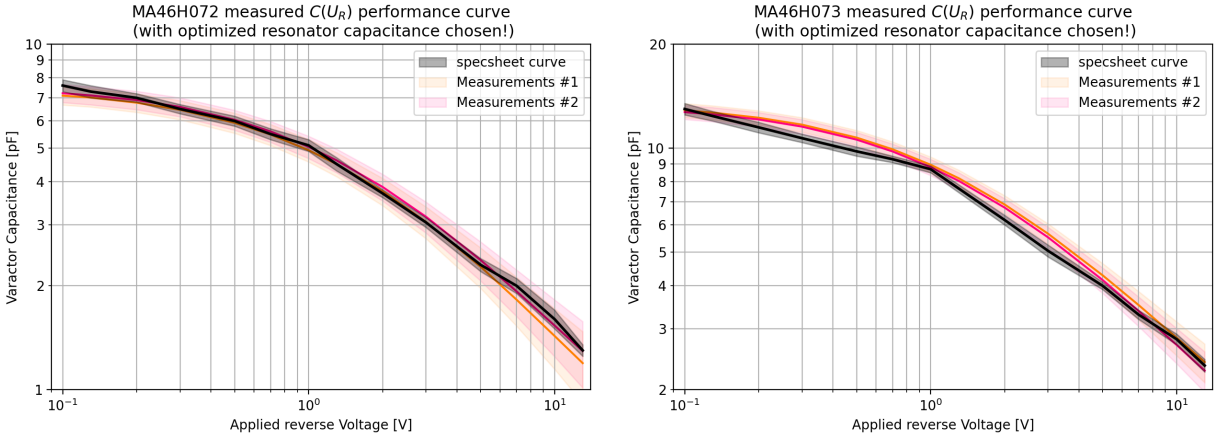

Figure 4: MA46H072-1056 / MA46H073-1056 room temperature characteristics.

3 High Voltage Characterizations

3.1 HV lines and HV switch testing

In the experiment, high voltage electrodes are needed for particle catching as even the decelerated antiprotons have a kinetic energy in the keV range which needs kV potentials to decelerate and trap. High voltage feedthroughs allow the externally applied voltage to reach the electrodes in the high voltage, high vacuum traps without leaks in the system, where it can produce the potential differences needed. Both components are surrounded by other components at less than 6 V of potential relative to ground. They are connected together and to the power supply by cables inside isolating PTFE tubes in grounded aluminium tubes to protect electronic circuits in the event of a spark. To test the voltage limits of the current experiment, a test setup with these three possible spark bottlenecks (see fig. 7) was built. Then, the HV lines were slowly pulled to an increasing potential with an ISEG SHR HV power supply until an electrical breakdown occurred or the maximum voltage of 6 kV was reached. The electrical breakdown was detected by letting the power supply trip above a current of 1 µA, which is a 33-fold increase over the 30 nA charging current at 10 V s^{-1} ramp up speed.

Trips consistently happened at 4.4(2) kV and were able to be localized to the electrode stack, which is not able to be changed without redesigning the trap stack. At less than 2 mm distance between the electrodes, with a relatively sharp edge and a breakdown voltage of 30 kV mm^{-1} in perfectly dry air, this seems reasonable. Both other components were able to reach the maximum 6 kV on their own, so the HV line isolation is fully sufficient in their current form. At vacuum pressure of 1×10^{-6} mbar, breakdown voltages increase by orders of magnitude as stated in Paschen's law. The increase is counteracted by the electron clouds in the trap and localized outgassing, but only to a smaller degree. Thus, we can conclude that 4 keV particles are able to be caught with the experiment in its current form.

At 4 keV, antiprotons need 114 ns to cross the 5cm space of the reservoir trap between the two high voltage electrodes from the degrader, including reflection. In this time, the front

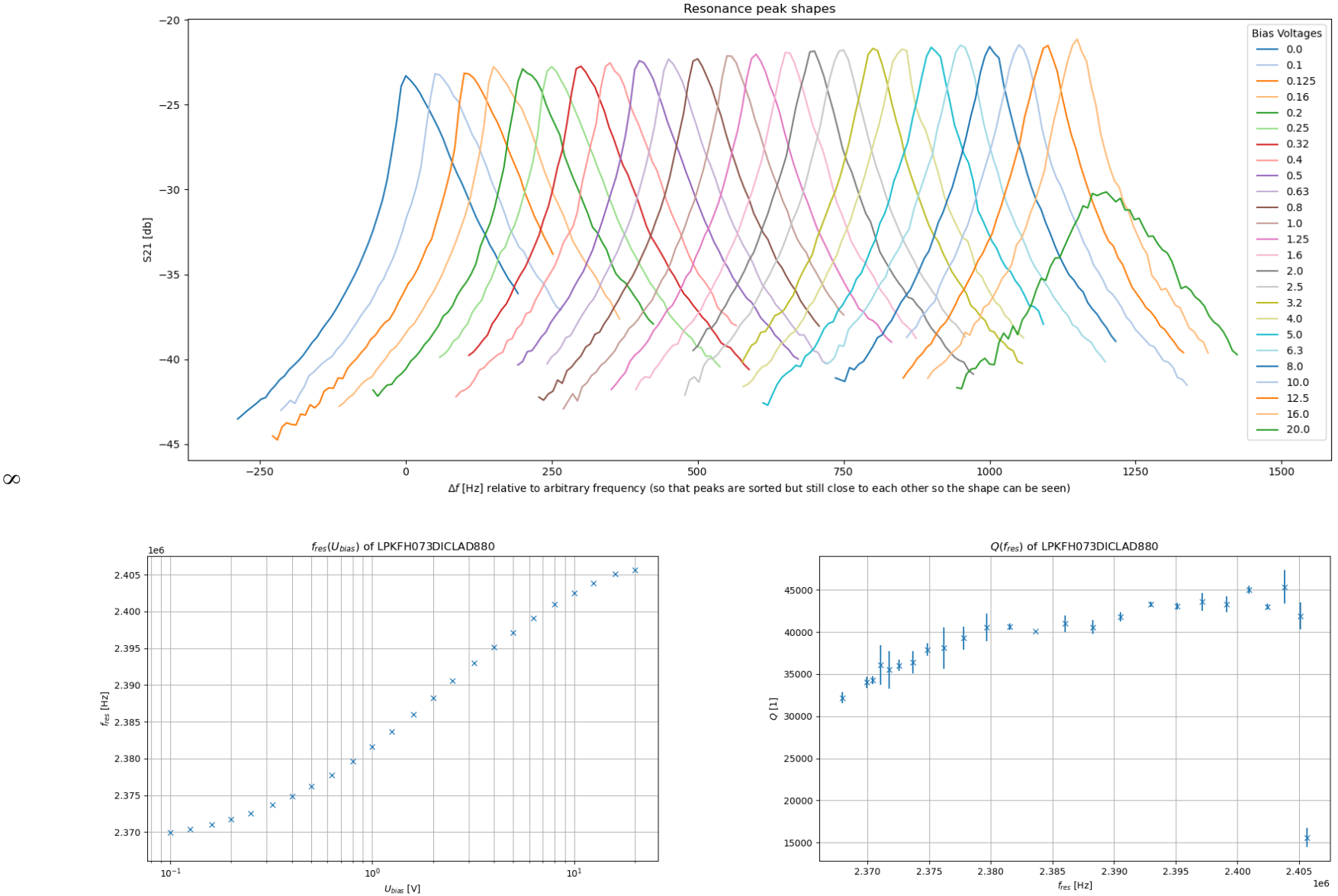

Figure 5: MA46H073-1056 Varactor board behaviour at 3 K

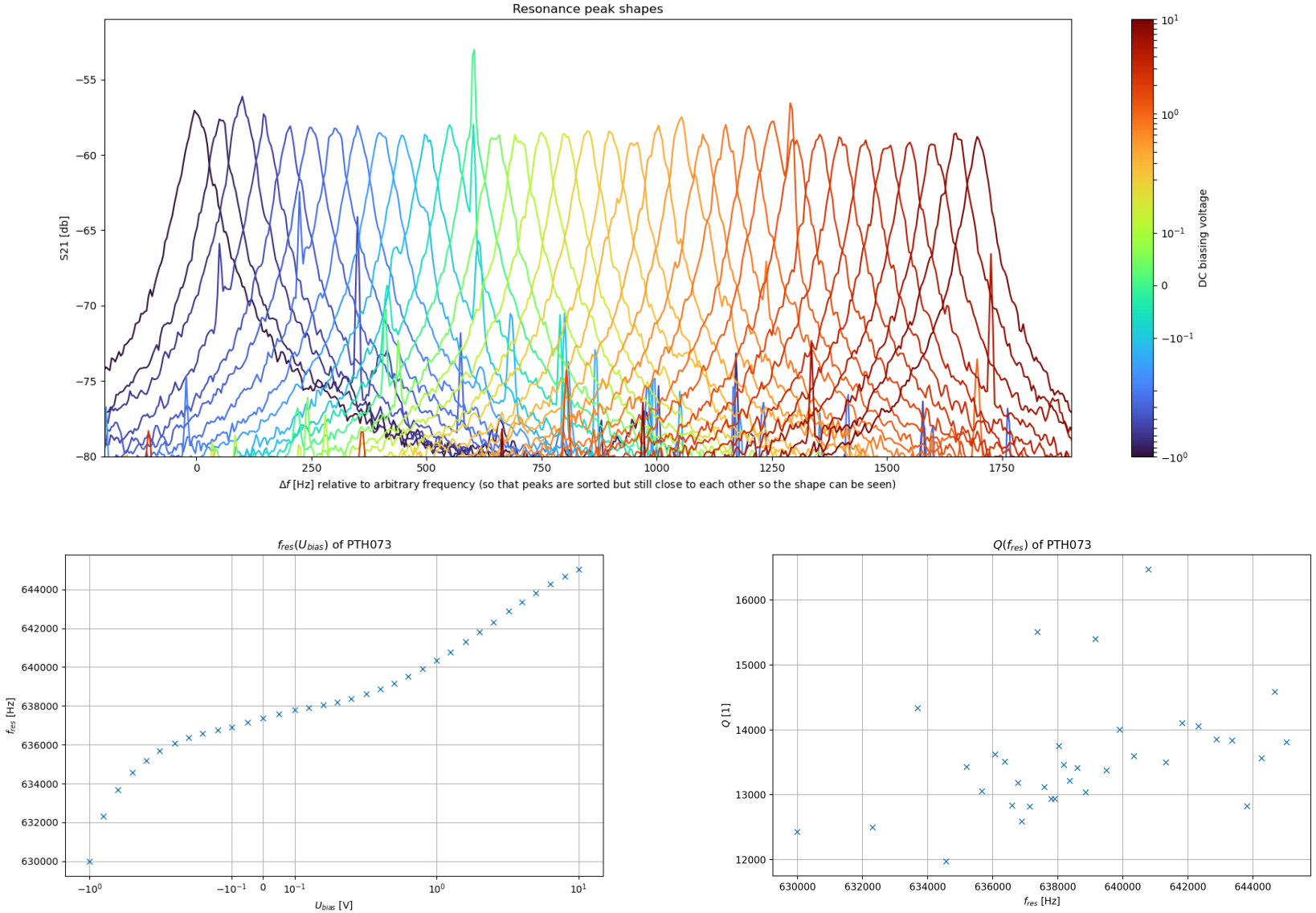

Figure 6: MA46H073-1056 Varactor board behaviour at cryogenic temperature, connected to the precision trap

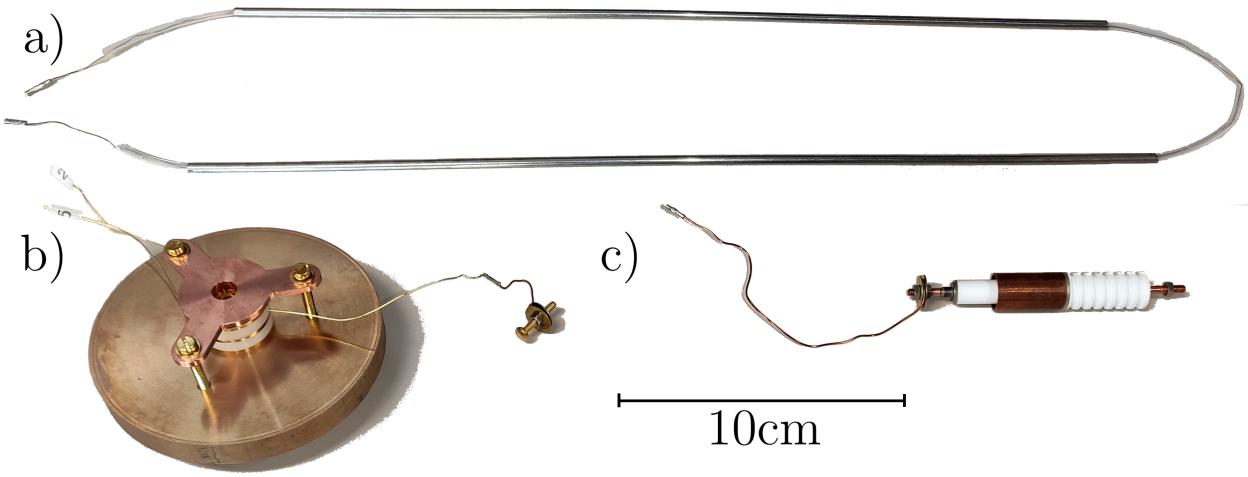

Figure 7: Components of the HV test setup. a) HV lines, b) HV electrodes, c) HV feed-through. In the test setup, they were connected together and every other conducting part was grounded. 10cm

high voltage electrode needs to be pulled from ground potential to the 4 kV. Preferably in less time, to catch more of the antiprotons in the edges of the spacial distribution. A Behlke GHTS60 high voltage switch was Investigated for these properties together with the ISEG SHR HV power supply, an SRS delay generator and a Keysight MSOX3024T oscilloscope to record the switch behaviour. As can be seen in fig. 8, the switch needs roughly 130 ns after the external trigger until it starts switching in the intended direction. It starts preshooting in the opposite direction first from 100 ns to 130 ns, after which it reaches the input voltage after 30 ns to 70 ns, depending on its value. For low voltages (< 300 V), the relative ripple is larger and takes up to 600 ns until sufficiently decayed, while for high voltages (> 3500 V), relative ramp up speed decreases, reaching 70 ns to converge at 6000 V.

Switch reaction time can be compensated, as the external trigger is taken from ELENA with multiple hundred nanoseconds of lead over the antiprotons. It gets delayed before being fed to the HV switch, and this delay can be decreased if need. With a ramp time to 3000 V at 4000 V input voltage of less than 40 ns, and an insignificant preeshoot before, the Behlke GHTS60 qualifies as a suitable switch. Furthermore the noise characteristics of the switch were tested by hooking the output to a tektronix P6015A high voltage probe and the Keysight MSOX3024T, and the input again to the ISEG SHR HV power supply. fig. 9 shows that the oscilloscope dominated noise does not change noticeably when changing input voltage. Under assumption of insignificant noise at 0 V at both inputs, we can deduce that the nioise measured at 0 V comes from other components (mainly the oscilloscope). If their noise does not change at higher voltages, then the switch noise is insignificant for all voltages, because the noise shape stays constant. A further investigation with a signal analyzer provides no evidence to the contrary, showing the same noise spectrum independently of output voltage. This is important so the trapped particles do not get heated out.

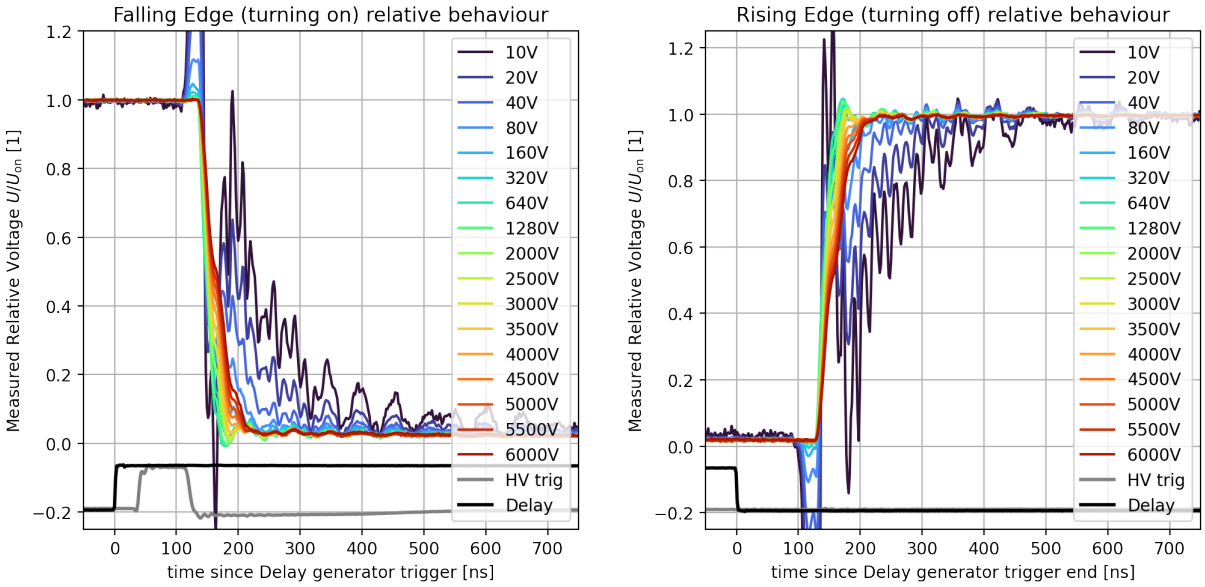

Figure 8: Behlke GHTS60 falling Edge (turn on) and rising Edge (turn off) behaviour

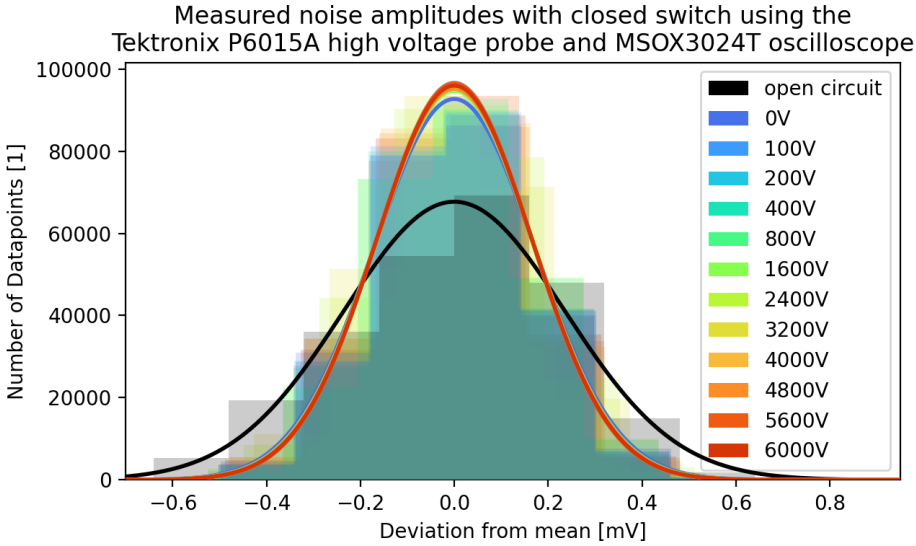

Figure 9: Noise values of the ISEG SHR, Behlke GHTS60, MSOX3024T, P6015A setup.

3.2 ISEG SHR LabVIEW Drivers

The ISEG SHR high precision high voltage power supply proved to be reliable enough to keep and use in the experiment. However, the BASE group is using LabVIEW to control and automate configuration and measurement with their appliances and the ISEG SHR does not support LabVIEW directly. It does, however, support SPCI programming via VISA over USB, which labview supports, too. So I programmed drivers on the basis of the SPCI communication analogous to those of other manufacturers. The resulting VI tree is shown in fig. 10.

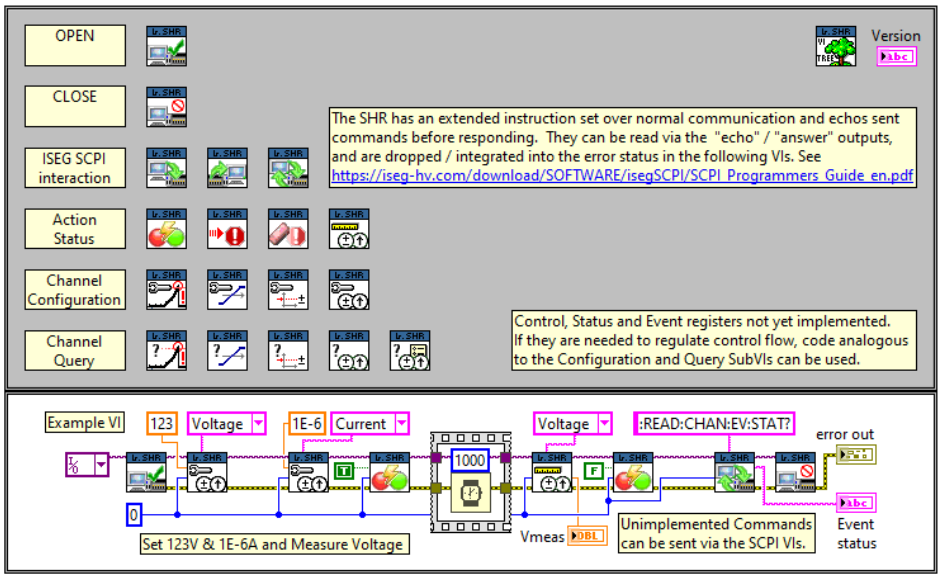

Figure 10: ISEG SHR LabVIEW driver for opening and closing the device connection, and for configuring, querying and measuring the device and its data.

Figure 11: Screwing of the BASE trapcan indium flange and drilling mounting holes for the medicine cabinet

4 Preparation of the Cryogenic Experiment

Aside from the specific projects, the BASE experiment needed to be opened up and closed down again (multiple times) to implement any intended changes and repair electrical components that turned out not to work after closing down the last time. These are multi day schemes consisting of multiple consecutive steps, some listed here in order for closing down:

The stack of Penning traps needs to be be inserted into a copper enclosure (trap can), which needs to be closed up with indium gaskets.

The closed trap can needs to be pumped out via a copper tube connection, and the connection needs to be pinched off afterwards.

Then, the closed trap can is screwed together with the rest of the 4 K stage, super-insulated and inserted into an aluminium tube (77 K stage).

It is then fastened inside the 77 K stage via Kevlar strings and aligned.

Each cryostat is connected to the respective stage and super-insulated.

Electronics are fed to their feedtroughs and connected before closing the experiment and tightening the flanges.

The experiment is leak-tested and cooled to 77 K before cooling further with liquid helium.

All electronics able to be tested at a certain stage of closing down also needs to be tested in this stage and the following stages, as a failure due to mishandling or ground contacts necessitates opening up again until the failure can be fixed. For opening up, the experiment needs to warm up over multiple days and then the steps need to be done in reverse order. I participated in these actions as an effectively equal member of the BASE team.

5 Smaller Projects

5.1 Manufacturing a Part

The brass bese in fig. 7 b) needed to be made so that the electrodes hat something to sit on. We also needed a cut down aluminium plate in the experiment as a floor to stand on. So I got to use the lathe, drill press and a circular saw.

5.2 Superconducting Magnet B-field Measurements

After a possible quench of the superconducting magnet, we remeasured the axial and radial distribution of the magnetic field and determined that only the shimming coils quenched while the main coils stayed operational. The shimming coils were later reloaded.

5.3 Sefety Improvements

When screwing CF flanges and working with sharp or hot equipment, small accidents may happen. But we had no first aid kit in the BASE Zone, meaning that we needed to go to another first aid kit in the Antimatter Decelerator Hall if something was needed. In the event of anything more serious than small cuts, this costs valuable time, so I bought, attached and filled a medicine cabinet in our Zone.

References

[1] Christian Smorra, Klaus Blaum, L Bojtar, M Borchert, KA Franke, T Higuchi, N Leefer, H Nagahama, Y Matsuda, A Mooser, et al. Base–the baryon antibaryon symmetry experiment. *The European Physical Journal Special Topics*, 224(16):3055–3108, 2015.

[2] Lowell S. Brown and Gerald Gabrielse. Precision spectroscopy of a charged particle in an imperfect penning trap. *Phys. Rev. A*, 25:2423–2425, Apr 1982.

[3] Lowell S. Brown. Line shape for a precise measurement of the electron's magnetic moment. *Phys. Rev. Lett.*, 52:2013–2015, Jun 1984.

[4] Matthias Borchert. *Challenging the Standard Model by high precision comparisons of the fundamental properties of antiprotons and protons.* PhD thesis, Gottfried Wilhelm Leibniz Universität Hannover, 2021.

[5] T. Tanaka. Development of tunable single particle detection system for an improved measurement of proton-to-antiproton charge-to-mass ratio. Master's thesis, University of Tokyo, 2016.

[6] Takashi Higuchi. *Development for an improved comparison of proton-to-antiproton charge-to-mass ratio.* PhD thesis, University of Tokyo, 2018.